Cold compaction of water ice

William B. Durham,[1] William B. McKinnon,[2] and Laura A. Stern[3]

Received 12 May 2005; revised 28 June 2005; accepted 25 July 2005; published 23 September 2005.

[1] Hydrostatic compaction of granulated water ice was measured in laboratory experiments at temperatures 77 K to 120 K. We performed step-wise hydrostatic pressurization tests on 5 samples to maximum pressures P of 150 MPa, using relatively tight (0.18–0.25 mm) and broad (0.25–2.0 mm) starting grain-size distributions. Compaction change of volume is highly nonlinear in P, typical for brittle, granular materials. No time-dependent creep occurred on the lab time scale. Significant residual porosity ($\sim$0.10) remains even at highest P. Examination by scanning electron microscopy (SEM) reveals a random configuration of fractures and broad distribution of grain sizes, again consistent with brittle behavior. Residual porosity appears as smaller, well-supported micropores between ice fragments. Over the interior pressures found in smaller midsize icy satellites and Kuiper Belt objects (KBOs), substantial porosity can be sustained over solar system history in the absence of significant heating and resultant sintering. **Citation:** Durham, W. B., W. B. McKinnon, and L. A. Stern (2005), Cold compaction of water ice, *Geophys. Res. Lett.*, *32*, L18202, doi:10.1029/2005GL023484.

1. Introduction

[2] Porosity and porosity evolution in meteorites and small solar system bodies such as asteroids have received considerable attention in recent years as asteroid densities have been determined with increasingly good resolution [*Britt et al.*, 2002]. In the outer solar system, substantial porosities (10s of %) have been postulated for comets [e.g., *Weissman et al.*, 2005], midsized icy satellites such as Mimas [*Eluszkiewicz*, 1990; *Eluszkiewicz et al.*, 1998], and KBOs [e.g., *Sheppard and Jewitt*, 2002]. All these bodies are thought to be predominantly composed of water ice, and represent a very large range in internal pressures and thermal and collisional histories. The pressures and temperatures experienced by midsized icy satellites and larger KBOs are substantial enough, however, to in principle reduce or eliminate porosity retained from accretion or created during later collisions [*McKinnon*, 2002]. Nevertheless, the experimental database upon which to construct an understanding of porosity and its evolution in ice and ice-rock bodies in the outer solar system is incomplete.

[3] A series of piston-cylinder compression experiments on cold, granular water ice, and in some cases mixtures of ice and rock grains, was undertaken by *Leliwa-Kopystynski and Maeno* [1993], *Leliwa-Kopystynski et al.* [1994], and *Leliwa-Kopystynski and Kossacki* [1995]. Temperatures varied considerably during many of those experiments, reaching levels of 213 K or higher. For one of the studies the minimum compression obtained, 80 MPa, was large, outside the range expected in of all but the largest midsized icy satellites and KBOs. Hydrostatic pressure in MPa as a function of radial distance r km within a sphere of uniform density ρ kg/m^3 and surface radius R km is

$$P = 1.4 \times 10^{-4}(\rho R)^2 \cdot \left(1 - r^2/R^2\right), \tag{1}$$

so the central pressure in a 1000-km diameter uniform sphere of ρ = 1500 kg/m^3 is about 80 MPa. Given these complexities, along with the slightly non-hydrostatic nature of stress in their piston cylinder apparatus, we determined to establish a "baseline" for the porosity that could be sustained in cold outer solar system bodies under hydrostatic pressure alone. Each body in the outer solar system has experienced a stochastic, and to some degree uniquely individual accretional, collisional, and thermal history. But whatever the individual history, the porosity structure today must be compatible with the limits imposed by pressure-driven compaction of cold ice-rock rubble.

2. Experiments

[4] Our objective here was to measure hydrostatic compaction, that is, the pressure-volume relationship, of granular ice I at low temperatures. We tested 5 samples; conditions and results are given in Table 1. Most (4 of 5) runs were conducted on the same initial size distribution of ice granules (0.18–0.25 mm) and most (4 of 5) were conducted at temperature T = 77 K. For one run the size range of the granules was wider: 0.25–2.0 mm, and for one run T was higher: 120 K. The wider range of grain sizes was used to achieve a lower starting porosity and warmer T was invoked to look for effects of creep. It was unclear at the start of testing if ductile flow would play a significant role in compaction at very low temperatures, because direct measurement of ductile strength of ice at T < 150 K is technologically out of the reach of conventional laboratory experiments. Compaction, however, may show a sensitivity to subtle amounts of creep not detectable by conventional strength testing. If the sample compressed at 115 K compacted more than a similar sample compressed at 77 K, all other conditions being identical, then we could infer that creep does assist compaction at 115 K. We might then be motivated to study time-dependent effects in compaction of KBOs and midsized icy satellites.

[5] The overall strategy was to prepare and compact the samples at low T and high pressure by the same general methods followed in our creep experiments on icy materials

[1]Lawrence Livermore National Laboratory, University of California, Livermore, California, USA.
[2]Department of Earth and Planetary Science, Washington University, St. Louis, Missouri, USA.
[3]U.S. Geological Survey, Menlo Park, California, USA.

0094-8276/05/2005GL023484$05.00

Table 1. Run Conditions and Results

Run	Particle Size (mm)	T(K)	Total Mass (g)	ϕ Initial	P Max (MPa)	ϕ Final
501	0.18–0.25	77	18.5 ± 0.2	0.46 ± 0.02	35	0.18 ± 0.04
502	0.18–0.25	77	17.9 ± 0.2	0.47 ± 0.02	80	0.12 ± 0.04
503	0.25–2.0	77	22.8 ± 0.2	0.37 ± 0.03	150	0.09 ± 0.03
504	0.18–0.25	120	20.1 ± 0.2	0.45 ± 0.02	100	0.12 ± 0.04
512	0.18–0.25	77	18.4 ± 0.2	0.43 ± 0.02	120	0.14 ± 0.04

[e.g., *Durham et al.*, 2003], the main difference being that the load applied here was purely hydrostatic (gas or liquid N_2) rather than hydrostatic plus deviatoric. The starting and ending shapes of the samples were always right cylindrical (Figure 1), suggesting that compaction was uniform throughout the sample and that the assumption of strain uniformity was sound.

2.1. Sample Preparation

[6] The five samples were prepared in a similar manner. The starting material was frozen from gas-free, triple-distilled water, then ground in a blender, sieved, and size fractions separated. Working in a freezer at approximately 245 K we spooned and lightly tamped portions of granulated material ~3 g at a time into soft, cylindrical indium "cans". The cans were then sealed to the pressure plug of the vessel. A central hole through the plug to the interior of the can allows internal pressure to be vented to atmosphere while the sample itself is sealed against external pressure by the indium encapsulation.

2.2. Experiments

[7] Generally, the same protocol was followed for each experiment. Samples were tested within 1 to 2 days of preparation. Cooling from freezer temperature to run T took place in the pressure vessel. Once T had stabilized, we proceeded with pressurizing the sample in steps up to maximum P, a process that took approximately two hours. Details of the pressurization sequence for each run are shown in the inset to Figure 2. Because the change of volume with pressure is more pronounced at lower pressures, we tended to increase the rate of pressurization as pressure increased. Except in one instance where the sample was held under pressure overnight, the vessel was then depressurized without delay, and the sample removed and stored. Samples 501–504 were stored in the freezer at 245 K; sample 512 was stored at 77 K after SEM revealed that grain shapes in 501–504 were strongly affected by the warmer freezer T.

[8] We measured the length of samples under pressure with good precision using the creep equipment associated with the apparatus, namely an axial moving piston and an internal force gage. When the moving piston contacts the bottom (free) end of the sample, a small force is registered on the internal force gage. The piston position is monitored by external transducers, so when the vessel is further pressurized and compaction causes the sample to shrink away from the end of the piston, the piston can be advanced to the new point of contact, and the change in length of the sample thus determined. At zero confining pressure, the force of the piston probably deforms the sample a small amount, which can be ignored. This technique was first used by *Heard and Page* [1982] to measure thermal expansivity of rocks under pressure.

3. Results

[9] Initial and final values of porosity ϕ, based on caliper measurements of sample length and diameter, are given in Table 1. For the 4 samples stored in the freezer after the experiments, we also measured final volume by Archimedes principle using cold ethanol as the displaced fluid. The agreement between the two measurement techniques was good, and the values of ϕ final in Table 1 for these 4 samples are the average of measurements using each technique. Estimated measurement errors are given in Table 1.

[10] Compaction curves for the 5 runs are shown in Figure 2. We calculated porosity during the runs based on the values of ϕ initial and ϕ final (Table 1) and an assumed linearity of porosity vs. measured sample length. That linearity requires uniform (but not necessarily isotropic) volume strain (supported by Figure 1 as discussed above) and no change in the pattern of volume strain with P. The error bars in Figure 2 are the uncertainty in ϕ final from Table 1, so refer to the entire curve. The relative uncertainty along any given curve is thus that of the length measurement (equivalent of porosity uncertainty ± 0.005 or better) plus the unquantified uncertainty in the above assumption of strain uniformity.

[11] Regarding the question of time-dependent ductile creep, sample 504, tested at 120 K, has a compaction curve that is indistinguishable from those of the other three samples of 0.18–0.25 mm ice, all tested at 77 K. Additionally, sample 503 was left under a pressure of 50 MPa for 12 hours after the original compaction measurements as it warmed to 125 K. The sample showed no further change in length from that measured at the conclusion of the original pressurization

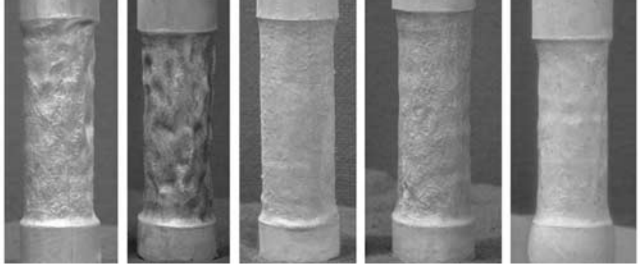

Figure 1. (left to right) Samples 501, 502, 503, 504, 512, after testing. Compacted ice samples are still inside the 0.5-mm-thick indium encapsulation. For scale, the diameter of the end caps is 26.4 mm.

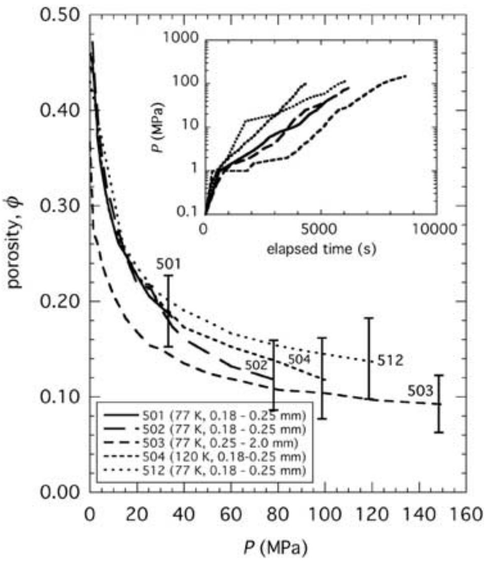

Figure 2. Compaction of ice. Porosity is corrected for the elastic effects of pressure on volume. The error bars shown represent the absolute uncertainty in porosity at the end of each run. Absolute errors in starting porosity are ±0.020 to 0.025 and are not plotted. We estimate relative uncertainty of porosity along any given curve as $\sim\pm 0.005$. Inset shows pressurization rates for each run. Note the logarithmic scale on the vertical axis, indicating that we increased the rate of pressurization with increasing pressure.

sequence. Seeing no signs of time or temperature dependence, we conclude that the primary mechanism of compaction in these tests is brittle fracture.

[12] Sample 503 with the wider range of granule size started with lower porosity, as expected when spheres of different diameter are packed together, and ended with lower porosity.

4. SEM Observations

[13] Fracture surface sections of compacted samples were prepared for SEM in a Gatan Alto 2100 cryo-preparation and coating station attached to the sample chamber of a LEO 982 field emission SEM. Specimens were held under vacuum at $T < 100$ K at all times during preparation, transfer, and examination.

[14] Grains in the starting material are equant to semi-equant with edges and corners rounded as well as angular. Sintering of grains is evident in SEM only after several days at freezer temperature, which compares with the 1–2 days between preparation and compaction of our samples.

[15] Sample 512, the only sample stored at 77 K following the run, shows evidence of brittle compaction (Figure 3). Shards of ice and a groundmass of particles of indistinguishable shape fill nearly all space between larger grains. Cracks are apparent at all scales, and are generally of high aspect ratio (i.e., nearly closed) and lie at random orientations. Stress fractures associated with depressurization do occur in some brittle materials, but in our experience those tend to be much longer and more widely spaced than those in Figure 3, so we believe that most were created under pressure. It may be impossible to determine directly the amount of porosity in sample 512 based on SEM images (e.g., by point counting). However, serendipitous information on residual porosity was provided by samples 501–504, which were stored for several months at 245 K between testing and SEM observation. Figure 4 shows a section through sample 503, taken to the highest pressure in this study. Sections from sample 512 and later stored at 245 K for approximately 2 months also took on the appearance of the material in Figure 4. Sintering at this relatively warm temperature has evidently allowed the porosity to coalesce into the lower-energy configuration of fewer, larger pores. We did not do a quantitative porosity measurement based on these images, but assert that the porosity visible in Figure 4 is consistent with the $\sim$0.1 of residual porosity for these two samples indicated in Figure 2.

5. Discussion and Conclusions

5.1. Interpretation

[16] All 5 water ice samples, hydrostatically compacted to pressures up to 150 MPa at 77–120 K, showed nonlinear porosity reduction with increasing pressure and residual porosities after highest pressurization of at least 0.10. The existence of significant residual porosity is further supported by the continued downward trends of the extensions

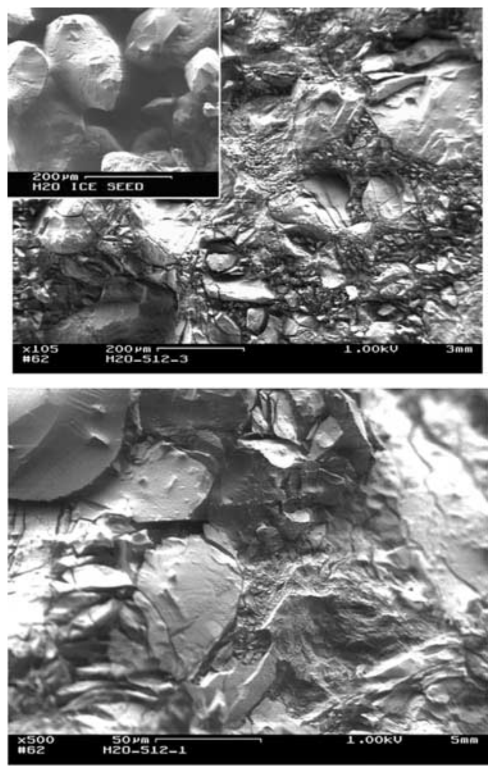

Figure 3. SEM images at 2 magnifications of a fracture section through sample 512, the only sample not allowed to sinter following testing. Some grains in the upper image have diameters near those of starting grains, while some grains are too small to be resolved even in the lower image. Fracture orientations in lower image are random. Inset in upper image (at same magnification as upper image) shows typical starting material.

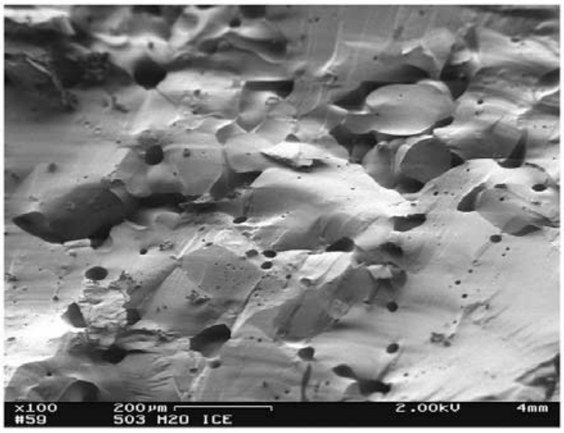

Figure 4. SEM image of sample 503, stored at 245 K for several months following testing. Sintering and annealing have caused the pores to coalesce, and allowed pore volume to be more easily calculated.

of the curves in Figure 2 and by SEM imaging (Figures 3 and 4).

[17] The nonlinear behavior we observe (Figure 2) is typical of granular materials [*Karner et al.*, 2003] and sums three basic processes: grain rearrangement without fracturing, more active at lowest pressures; grain failure at higher pressures; and Hertzian elastic deformation at all pressures [*Hagerty et al.*, 1993; *Karner et al.*, 2003]. The grain rearrangement stage, ordinarily a concave downwards trend at lowest pressures, is not apparent in Figure 2, suggesting that grain failure begins at very low pressures of kPa levels or below. The random fracture orientations and high aspect ratio fractures we see in Figure 3 are mostly the result of "Hertzian fracture," or shattering at contact points [e.g., *Zhang et al.*, 1990a, 1990b]. *Borg et al.* [1960] also report random fracture orientation in quartz sand under hydrostatic pressurization. Particle size distribution in highly compacted material ranges from near starting size to near submicroscopic [*Borg et al.*, 1960; *Hagerty et al.*, 1993; *Zhang et al.*, 1990b] and is probably fractal [*McDowell et al.*, 1996], also consistent with what we see in Figure 3.

[18] Aside from the work discussed in the Introduction, there is little cold compaction data on ice with which to compare, although much work has been done on soils and other materials [see, e.g., *Karner et al.*, 2003, and references therein]. Quartz sand has been studied extensively and as a brittle material provides useful insight into crushing processes in cold ice. We infer from the lack of time- and temperature-dependent effects that compaction in cold ice is the result of brittle failure of granules, and scaling the crushing curves for ice and for quartz by brittle strength gives reasonably good support for this inference. Crush curves for quartz sand vary considerably depending on factors such as starting porosity and grain size distribution, but broadly differ from ours in Figure 2 by a factor of 20 [*Borg et al.*, 1960; *Karner et al.*, 2003; *Maxwell*, 1960]. This factor compares well to the ratio of unconfined brittle compressive strength for quartz at room T ($\sim$2 GPa, [*Borg et al.*, 1960]) to that for ice at T = 77 K MPa (50–150 MPa [*Durham et al.*, 1983]).

5.2. Implications

[19] Our experiments indicate substantial reduction in porosity in cold granular water ice (and by implication in cold ice or ice-rock rubble as long as the ice is volumetrically dominant) over a hydrostatic pressure range of $\sim$1–150 MPa. Somewhat surprisingly, substantial residual porosity ($\sim$0.10) persists at pressures in excess of 100 MPa, contained mostly in micropores supported by small shards of fractured material. We conclude that over the interior pressures found in midsize icy satellites and KBOs (Equation 1), non-negligible porosity can be sustained over solar system history in the absence of significant heating and sintering, annealing, and pore collapse. For smaller midsize icy satellites and KBOs, such as Phoebe, which are more likely to have remained cool, such porosity may be substantial and may be important in interpretation of bulk density measurements.

[20] **Acknowledgments.** Work by all authors was supported by grants from the NASA Planetary Geology and Geophysics Program. Work was performed under the auspices of the U.S. Department of Energy by the Lawrence Livermore National Laboratory under contract W-7405-ENG-48.

References

Borg, I., M. Friedman, J. Handin, and D. V. Higgs (1960), Experimental deformation of St. Peter sand: A study of cataclastic flow, in *Rock Deformation*, edited by D. Griggs and J. Handin, *Mem. Geol. Soc. Am.*, *79*, 133–191.

Britt, D. T., D. Yoemans, K. Housen, and G. Consolmagno (2002), Asteroid density, porosity, and structure, in *Asteroids III*, edited by W. F. Bottke et al., pp. 485–500, Univ. of Ariz. Press, Tucson.

Durham, W. B., H. C. Heard, and S. H. Kirby (1983), Experimental deformation of polycrystalline H_2O ice at high pressure and low temperature: Preliminary results, *J. Geophys. Res.*, *88*, 377–392.

Durham, W. B., L. A. Stern, and S. H. Kirby (2003), Ductile flow of methane hydrate, *Can. J. Phys.*, *81*, 373–380.

Eluszkiewicz, J. (1990), Compaction and internal structure of Mimas, *Icarus*, *84*, 215–225.

Eluszkiewicz, J., J. Leliwa-Kopystynski, and K. J. Kossacki (1998), Metamorphism of solar system ices, in *Solar System Ices*, edited by B. Schmitt, C. de Bergh, and M. Festou, pp. 119–139, Springer, New York.

Hagerty, M. M., D. R. Hite, C. R. Ullrich, and D. J. Hagerty (1993), One-dimensional high-pressure compression of granular media, *J. Geotech. Eng.*, *119*(1), 1–18.

Heard, H. C., and L. Page (1982), Elastic moduli, thermal expansion, and inferred permeability of granites to 350°C and 55 megapascals, *J. Geophys. Res.*, *87*, 9340–9348.

Karner, S. L., F. M. Chester, A. K. Kronenberg, and J. S. Chester (2003), Subcritical compaction and yielding of granular quartz sand, *Tectonophysics*, *377*(3–4), 357–381.

Leliwa-Kopystynski, J., and K. J. Kossacki (1995), Kinetics of compaction of granular ices H_2O, CO_2, and $(NH_3)_x$ $(H2O)_{1-x}$ at pressures of 2–20 MPa and in temperatures of 100–270 K—Application to the physics of icy satellites, *Planet. Space Sci.*, *43*, 851–861.

Leliwa-Kopystynski, J., and N. Maeno (1993), Ice/rock porous mixtures: Compaction experiments and interpretation, *J. Glaciol.*, *39*, 643–655.

Leliwa-Kopystynski, J., L. Makkonen, O. Erikoinen, and K. J. Kossacki (1994), Kinetics of pressure-induced effects in water ice/rock granular mixtures and application to the physics of icy satellites, *Planet. Space Sci.*, *42*, 545–555.

Maxwell, J. C. (1960), Experiments on compaction and cementation of sand, in *Rock Deformation*, edited by D. Griggs and J. Handin, *Mem. Geol. Soc. Am.*, *79*, 105–132.

McDowell, G. R., M. D. Bolton, and D. Robertson (1996), The fractal crushing of granular materials, *J. Mech. Phys. Solids*, *44*(12), 2079–2102.

McKinnon, W. B. (2002), On the initial thermal evolution of Kuiper Belt objects, in *Proceedings of Asteroids, Comets, Meteors (ACM 2002)*, *Eur. Space Agency Spec. Publ.*, *500*, 29–38.

Sheppard, S. S., and D. C. Jewitt (2002), Time-resolved photometry of Kuiper Belt objects: Rotations, shapes, and phase functions, *Astron. J.*, *124*, 1757–1775.
Weissman, P. R., E. Asphaug, and S. C. Lowry (2005), Structure and density of cometary nuclei, in *Comets II*, edited by M. Festou, H. U. Keller, and H. Weaver, pp. 337–357, Univ. of Ariz. Press, Tucson.
Zhang, J. X., T. F. Wong, and D. M. Davis (1990a), Micromechanics of pressure-induced grain crushing in porous rocks, *J. Geophys. Res.*, *95*, 341–352.
Zhang, J. X., T. F. Wong, T. Yanagidani, and D. M. Davis (1990b), Pressure-induced microcracking and grain crushing in Berea and Boise sandstones—Acoustic-emission and quantitative microscopy measurements, *Mech. Mater.*, *9*(1), 1–15.

W. B. Durham, Lawrence Livermore National Laboratory, University of California, Livermore, CA 94550, USA. (durham1@llnl.gov)
W. B. McKinnon, Department of Earth and Planetary Science, Washington University, St. Louis, MO 63130, USA.
L. A. Stern, U.S. Geological Survey, Menlo Park, CA 94025, USA.